nature nanotechnology

SUPPLEMENTARY INFORMATION

https://doi.org/10.1038/s41565-019-0558-z

In the format provided by the authors and unedited.

Origin of lithium whisker formation and growth under stress

Yang He[1], Xiaodi Ren[2], Yaobin Xu[1], Mark H. Engelhard[1], Xiaolin Li[2], Jie Xiao[2], Jun Liu[2], Ji-Guang Zhang[2], Wu Xu[2]* and Chongmin Wang[1]*

[1]Environmental Molecular Sciences Laboratory, Pacific Northwest National Laboratory, Richland, WA, USA. [2]Energy and Environmental Directorate, Pacific Northwest National Laboratory, Richland, WA, USA. *e-mail: wu.xu@pnnl.gov; chongmin.wang@pnnl.gov

Supplementary Information for

Origin of Lithium Whisker Formation and Growth under Stress

Yang He, Xiaodi Ren, Yaobin Xu, Mark H. Engelhard, Xiaolin Li, Jie Xiao, Jun Liu, Ji-Guang Zhang, Wu Xu, Chongmin Wang

Supplementary Information includes:

Supplementary Figures 1-10

Supplementary Discussion

Supplementary Video Captions 1-8

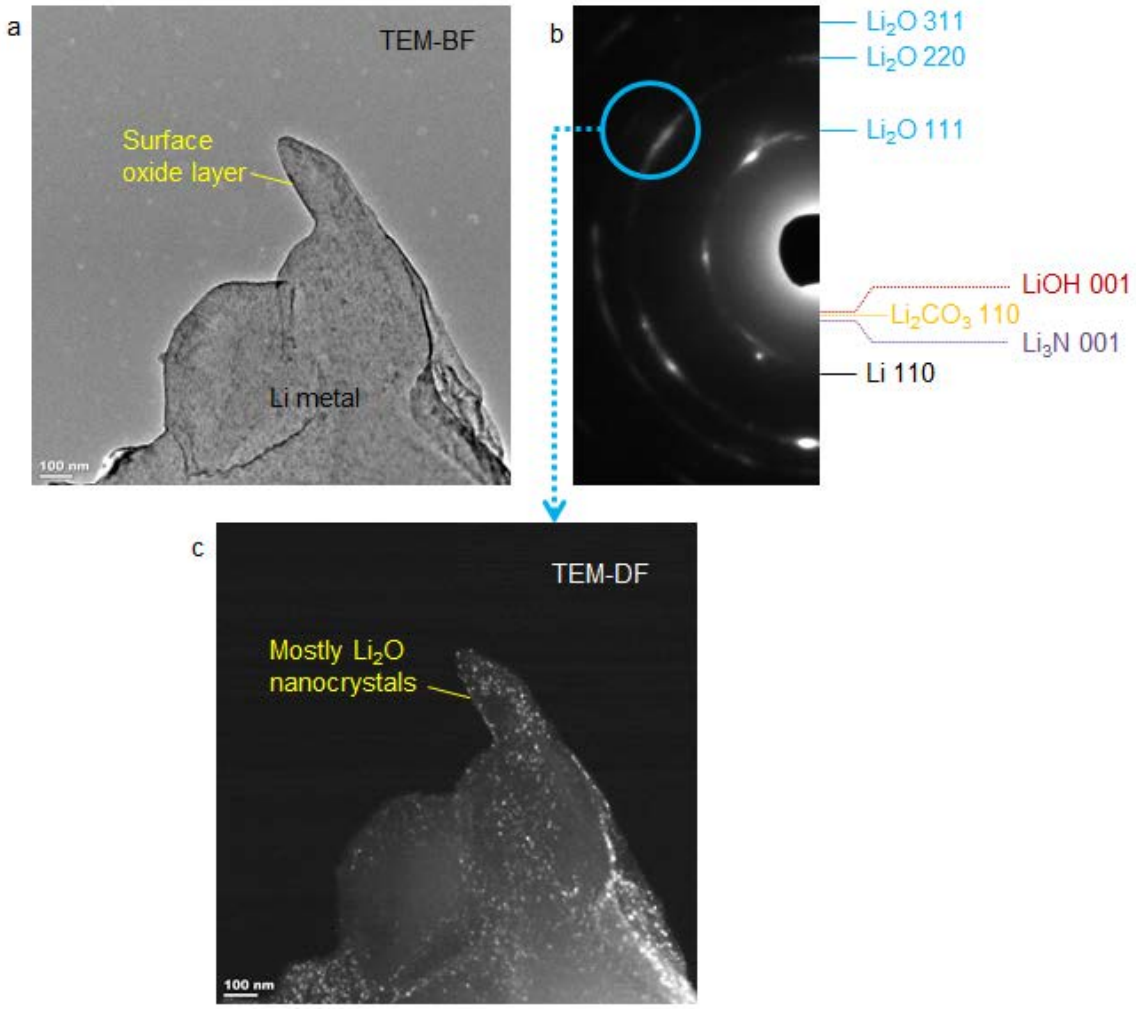

Supplementary Fig. 1 | Li_2O as the dominant surface species on the Li metal (counter-electrode) surface after exposure to air for ~5 seconds. a. TEM bright field (TEM-BF) image of the Li metal on the counter-electrode. **b.** Selected area electron diffraction pattern from panel (**a**), showing strong diffraction signals from Li metal and Li_2O, and weak diffraction signals which potentially can be assigned to Li_2CO_3, LiOH, and Li_3N. **c.** TEM dark field (TEM-DF) image using the Li_2O diffraction signals (circled region in panel (**b**)). This information demonstrates that the surface of Li metal on the counter electrode is covered primarily by Li_2O nanocrystals, with only trivial amount of Li_2CO_3, LiOH, and Li_3N.

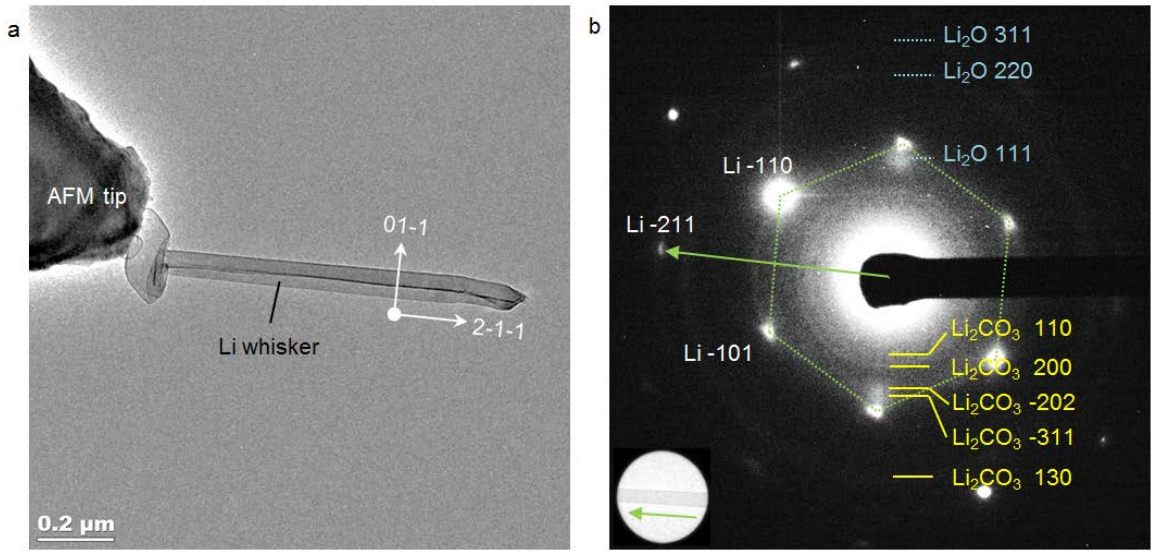

Supplementary Fig. 2 │ Electron diffraction analysis of the surface species and orientation of the Li whisker deposited in situ. a. TEM bright field image of the Li whisker. Arrows mark the crystallographic orientation of the whisker. Clearly, the whisker is primarily bounded by {1 1 0} surface facets. **b.** Electron diffraction of the whisker during its growth. Green hexagon indicates the symmetry of the Li <1 1 1> zone axis. Green arrow indicates the whisker length direction, i.e. <-2 1 1>. The additional diffraction rings can be assigned to Li_2CO_3 and Li_2O crystals. Inset shows the selected area of the growing whisker. Note that the orientation relation of Li surface and Li_2CO_3 shows a rough orientation relation of $(0\ 1\ -1)_{Li}$ // $(-2\ 0\ 2)_{Li2CO3}$.

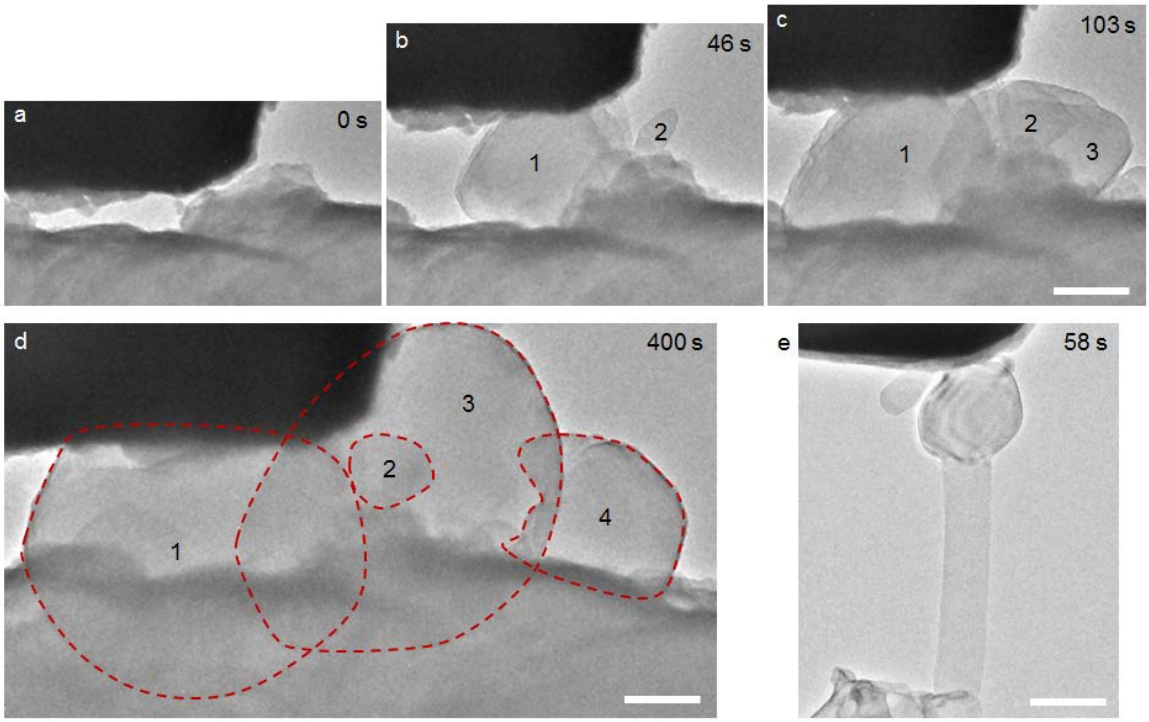

Supplementary Fig. 3 | Sequential TEM snapshots showing Li deposition process in ~10^{-2} mbar N_2 gas environment (a-d). The continuous expansion of the side surfaces (see Supplementary Video 2) indicates that the Li deposition was not localized at the Li whisker-electrolyte interface but occurred primarily on the side surfaces of these Li particles. Therefore, the electrochemical deposition in N_2 did not introduce Li whiskers terminated sharply by well-defined {1 1 0} surface facets. **e.** Li whisker formed in CO_2 environment, which is reproduced from Fig. 2f for comparison with the observation of large Li particles growing in N_2. Clearly, the Li deposition and morphology of the deposited Li are closely associated with the surrounding environment. Dash circles in (**d**) mark roughly the contour of the deposited Li particles. Spring constant of the AFM cantilever is ~3 $N \cdot m^{-1}$. Scale bars in (**c, d, e**) 200 nm. Note that multiple nucleation events took place simultaneously in most of the cases, likely due to the "underlying electronic connection" between these nucleuses. For example, other than enabling Li growth normal to the contact, electrons from the working electrode may also assist Li deposition tangential to the solid electrolyte surface; therefore, a thin film of Li metal could gradually form on the solid electrolyte surface, which originates from the contact and expand on the surface of the solid electrolyte. Then, electrons can be conducted to nearby surface, concentrate at sites where electric field is high, and consequently lead to "separated" deposition events. Note that the same set-up (same AFM tip and Li metal on the counter electrode) was used for Li deposition in a CO_2 environment (see Supplementary Figs. 6 & 9).

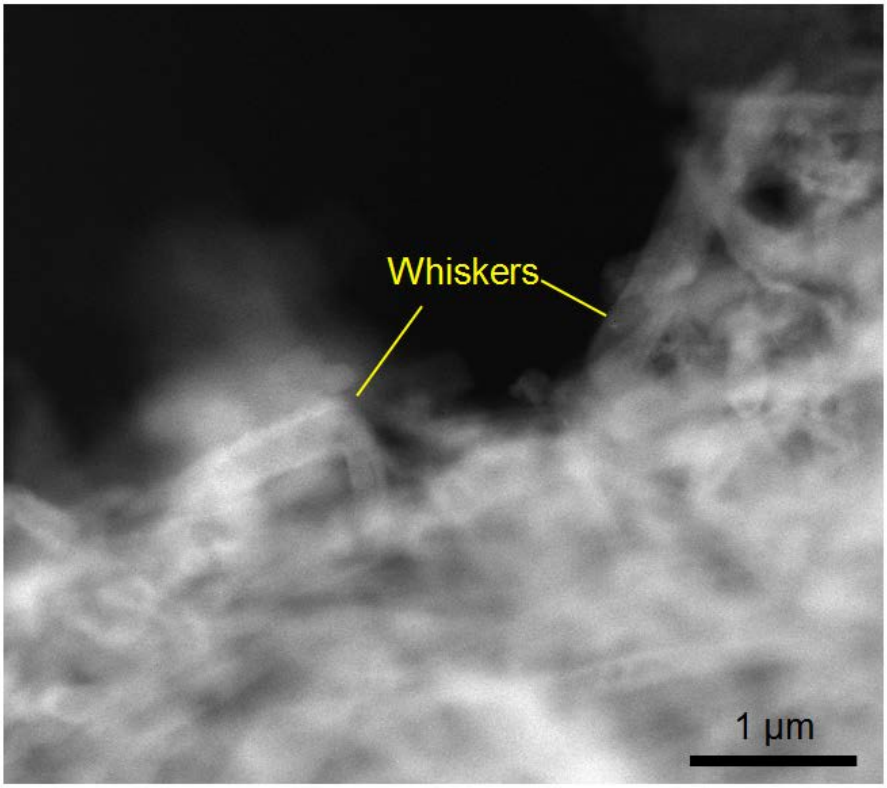

Supplementary Fig. 4 | Cryo-STEM image of Li whiskers. The cryo-STEM image reveals the extensive formation of Li whiskers following the poisoning of the base electrolyte with 2wt% ethyl methyl carbonate in a coin cell.

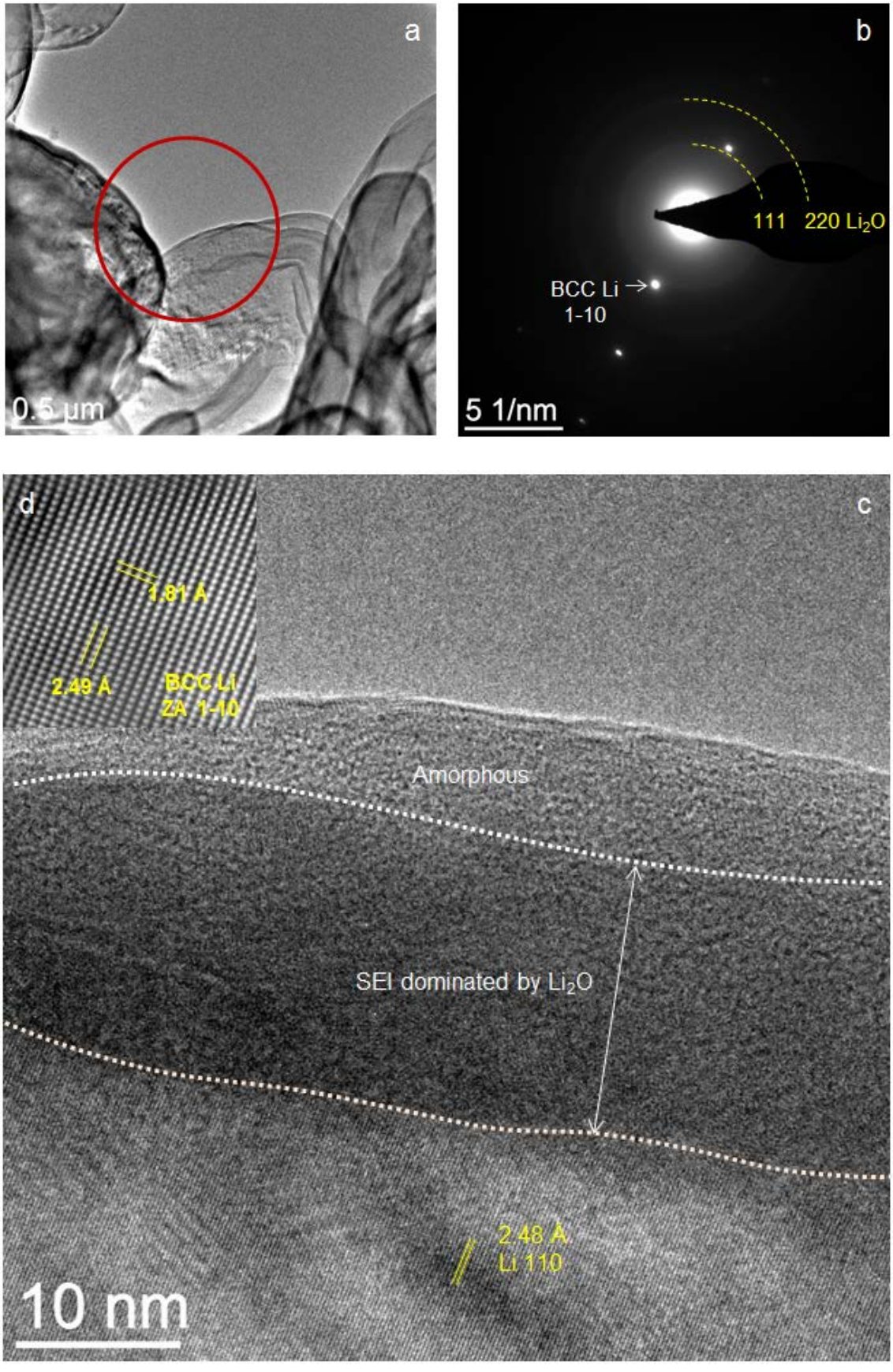
a
0.5 µm
b
111
220 Li2O
BCC Li
1-10
5 1/nm
d
1.81 Å
2.49 Å
BCC Li
ZA 1-10
c
Amorphous
SEI dominated by Li2O
2.48 Å
Li 110
10 nm

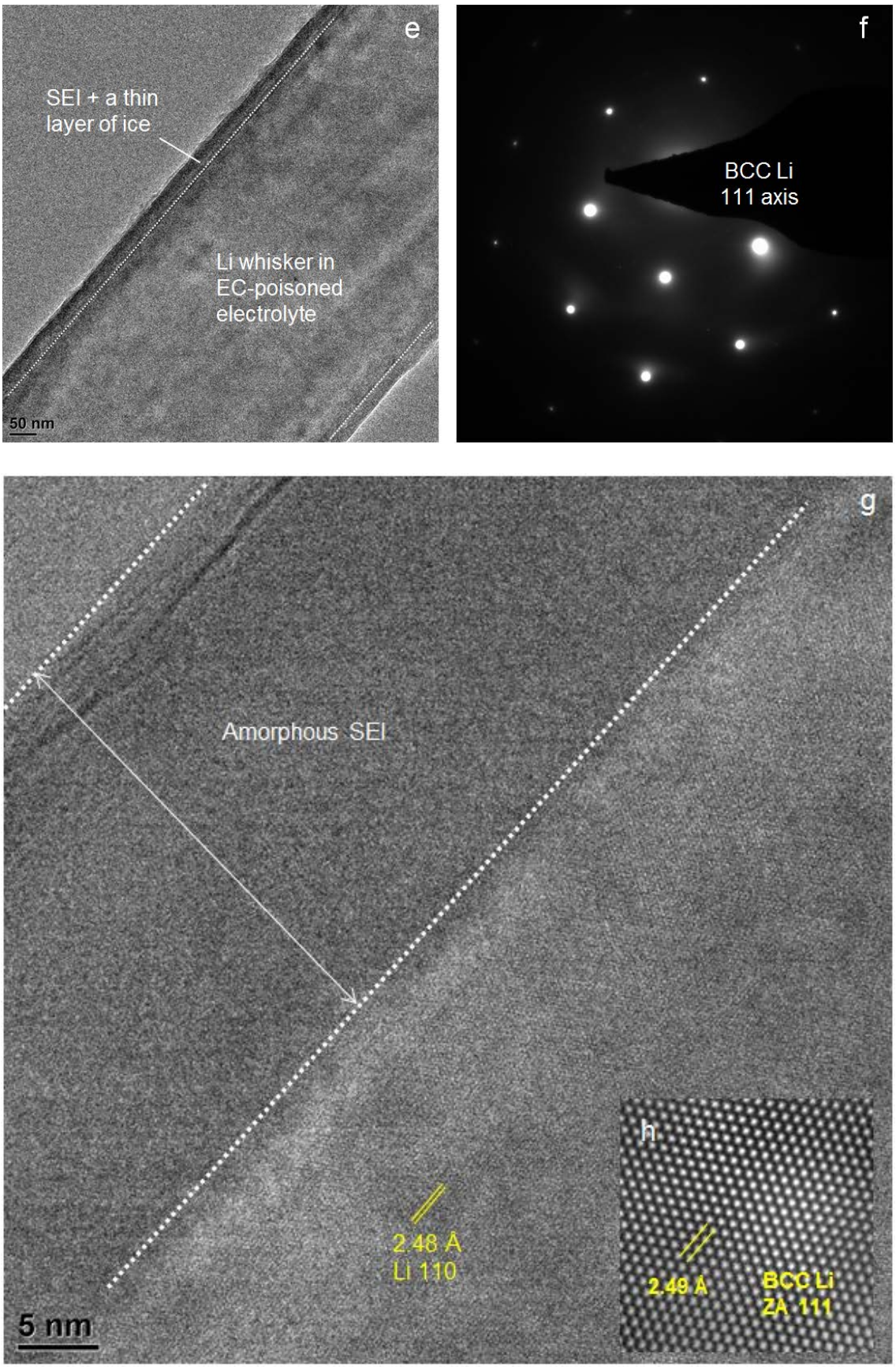
e
SEI + a thin
layer of ice
Li whisker in
EC-poisoned
electrolyte
50 nm
f
BCC Li
111 axis
g
Amorphous SEI
2.48 Å
Li 110
5 nm
h
2.48 Å
BCC Li
ZA 111

Supplementary Fig. 5 | Cryo-TEM and electron diffraction characterization of the deposited Li and the SEI formed in 2wt% cyclohexanone-poisoned (a-d) and 2wt% EC-poisoned (e-h) baseline electrolyte. a, e, Monolith and whisker morphology of the deposited Li, respectively. **b, f,** Selected area electron diffraction patterns of the deposited Li, showing clear evidence of Li_2O formation in cyclohexanone-poisoned electrolyte. **c, g,** High resolution cryo-TEM image showing the dominant Li_2O crystals in the SEI and amorphous phase dominated SEI, respectively. **d, h,** Filtered high resolution TEM image of the Li metal demonstrating the perfect BCC Li lattices.

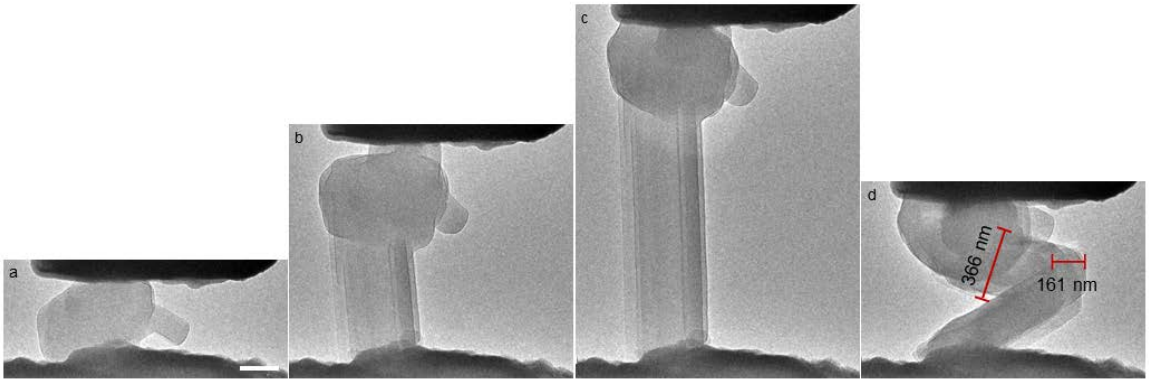

Supplementary Fig. 6 | Sequential TEM images showing the buckling behavior of a growing Li whisker. a. Nucleation, **b-c.** growth (driven by a constant voltage) and **d.** buckling of the Li whisker growing under the elastic constraint of an AFM cantilever (that mimics the separator). Based on the maximum deflection of the AFM cantilever (spring constant k ~3 N m^{-1}), the maximum force generated by the whisker growth (so-called "growth force") was 5586 nN. Based on the measured cross-sectional dimensions of the whisker (see panel (**d**)), the compressive stress at the point of buckling is ~95 MPa, which is well consistent with that calculated from Euler's formula ~92 MPa. See Supplementary Video 3. Scale bar in (**a**), 200 nm.

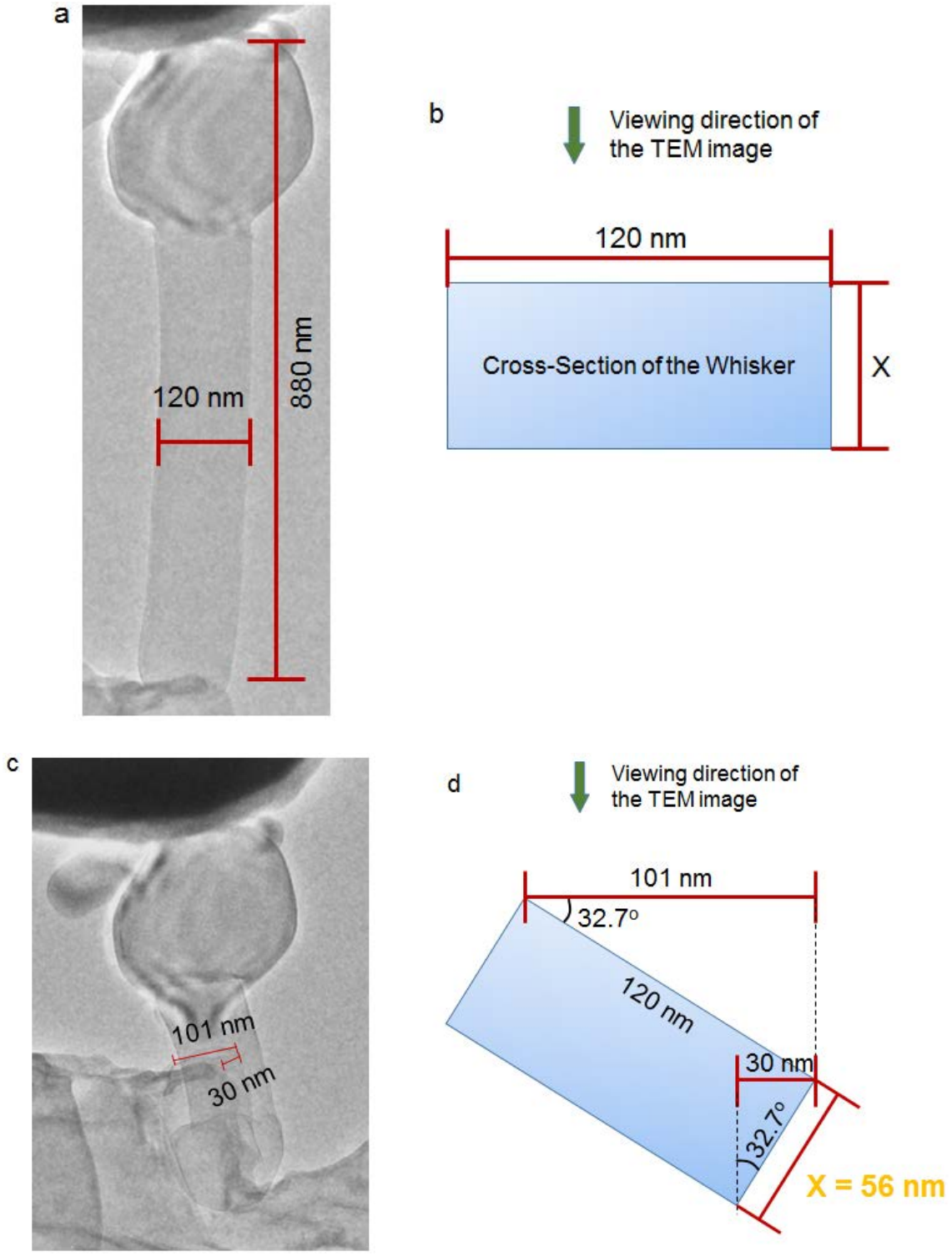

Supplementary Fig. 7 | Cross-sectional dimensions of the Li whisker in Fig. 2f. a. Reproduced Fig. 2f with measured width and length of the whisker. **b.** Schematic of the whisker's cross-section; thickness of the whisker is assumed to be X. **c.** Reproduced Fig. 2g showing a inclined view of the cross-section at the fractured region. **d.** Schematic of the inclined view of the

cross-section. Green arrows indicate the viewing direction of the TEM images. Based on these views, cross-sectional dimensions of the whisker can be determined. Based on the maximum deflection of the AFM cantilever (Fig. 2h), the growth force of the whisker is 352 nN; the corresponding compressive stress on the Li whisker upon buckling is ~52 MPa which is well consistent with that calculated from Euler's formula ~50 MPa.

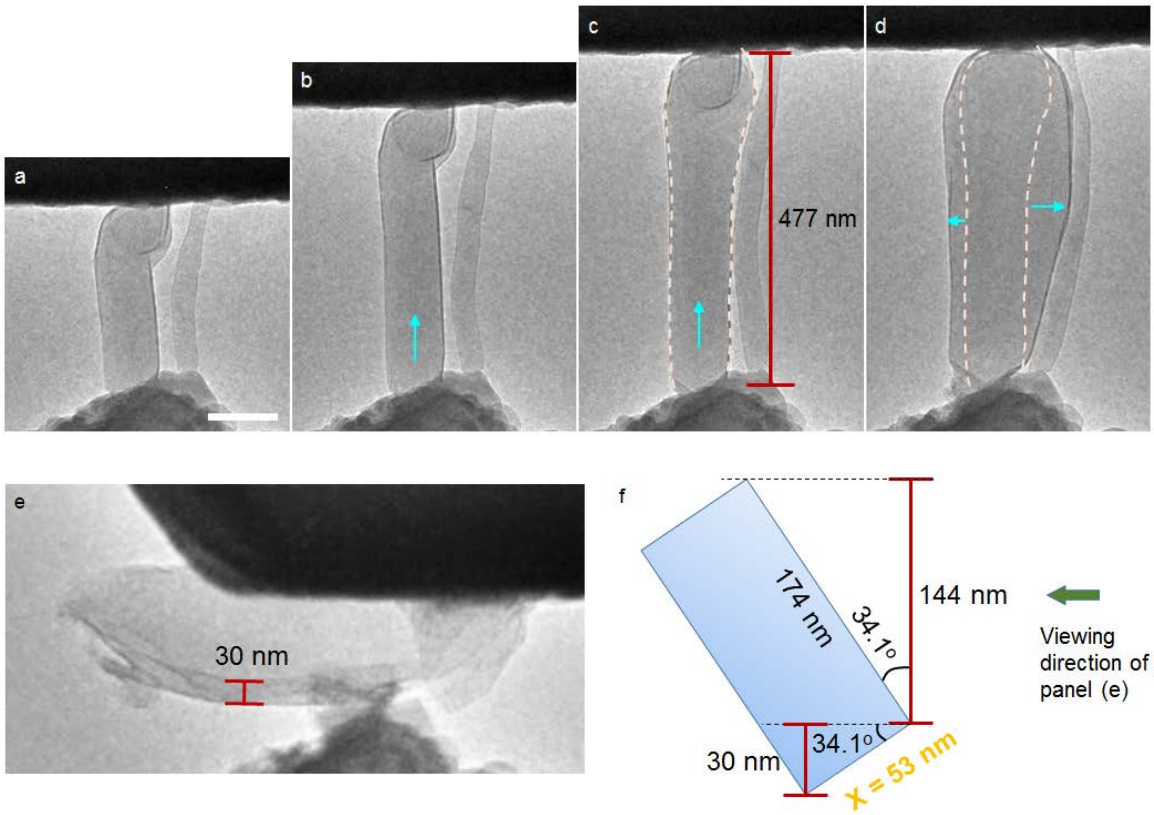

Supplementary Fig. 8 | Cessation of the (vertical) growth in length and subsequent lateral growth at constant length. a-d. Sequential TEM images showing Li whisker elongation, stop elongation, and lateral expansion. **e-f.** Inclined side-view of the Li whisker and cross-sectional dimensions analysis. Note that constant voltage was applied during the whisker growth and the spring constant of the AFM cantilever was ~0.1 N m^{-1}. The critical stress required to stop the deposition on the interface was measured to be ~13 MPa which was much lower than that required for buckling ~152 MPa. See Supplementary Video 6. Scale bar in (**a**), 100 nm.

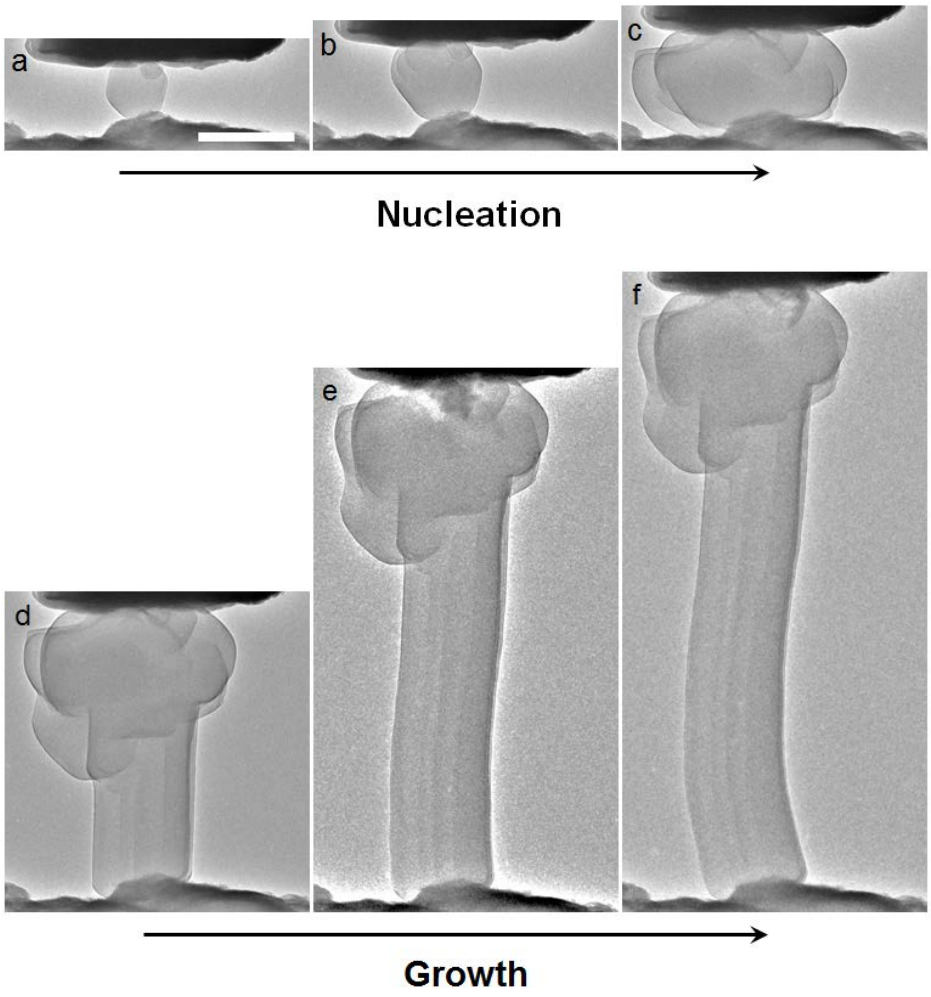
a
b
c
Nucleation
d
e
f
Growth
g
Yield
h
Buckling

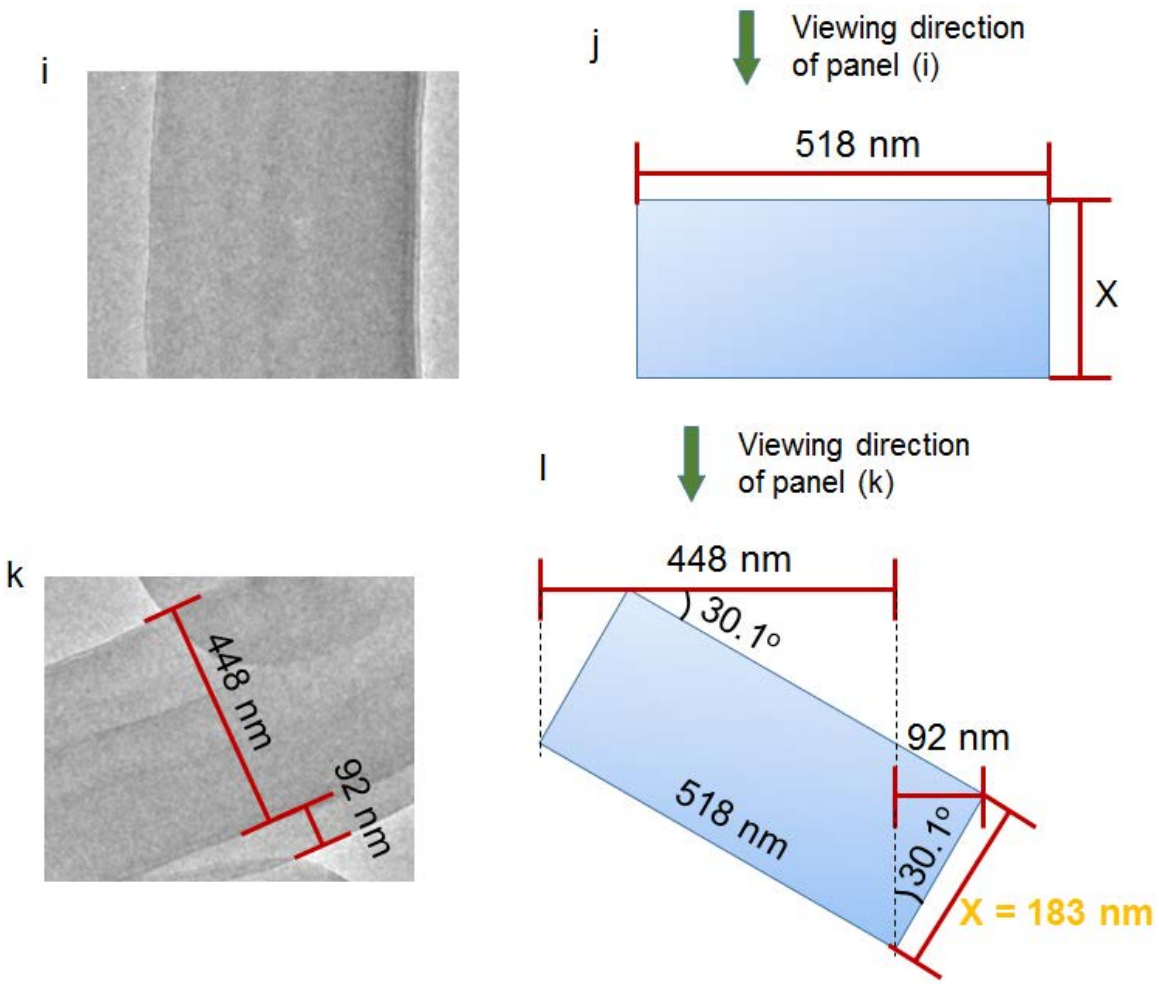

Supplementary Fig. 9 | Yielding of a growing Li whisker under stress. a-c. Sequential TEM images showing nucleation, **d-f.** growth, **g.** yielding and **h.** subsequent buckling, driven by a constant voltage. Based on the maximum deflection of the AFM cantilever, the growth force was 9453 nN. Based on the cross-sectional dimensions of the whisker (**i-l**), the corresponding compressive stress at the point of yielding is ~100 MPa which is roughly consistent with the yield strength of small scale Li metal and slightly larger than that calculated from Euler's formula ~85 MPa. Therefore, the initiation of buckling before yielding did not immediately result in collapse of the Li whisker. See Supplementary Video 8. Scale bar in (**a**), 500 nm.

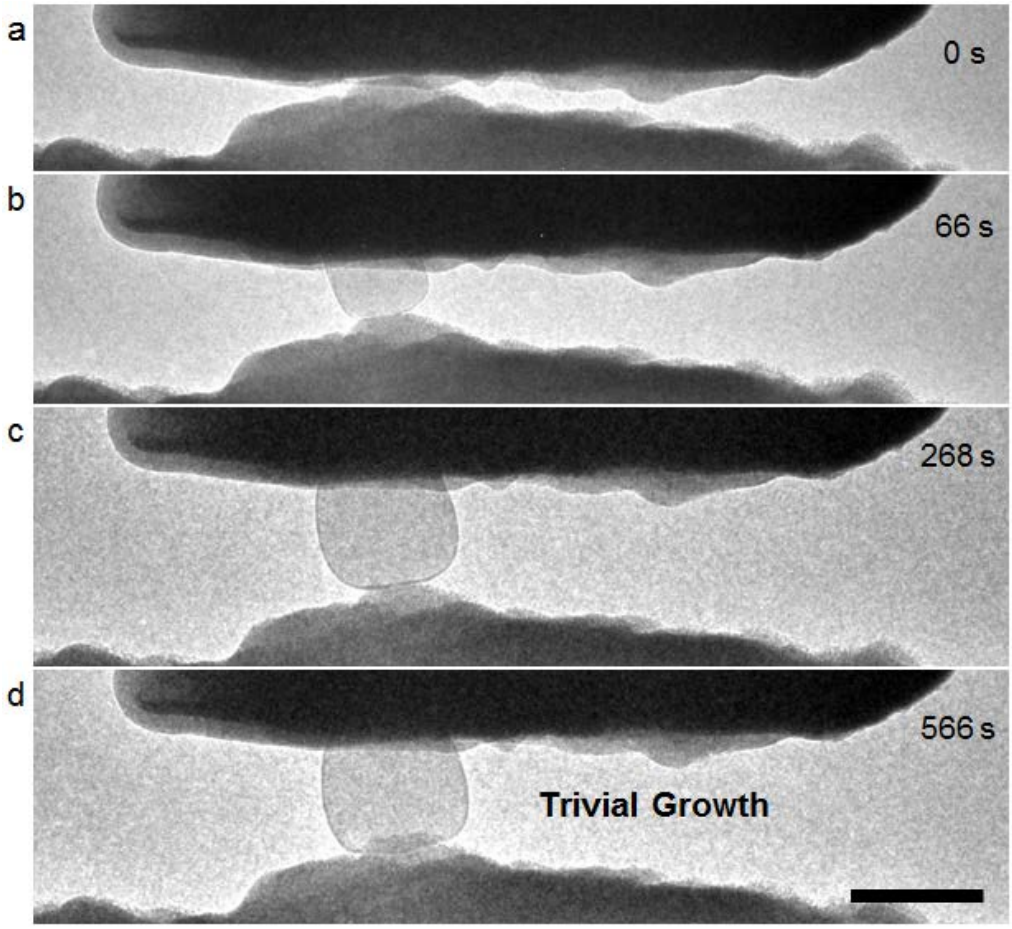

Supplementary Fig. 10 | Li deposition process in ~10^{-2} mbar CO_2 environment under a stiff AFM cantilever. Spring constant of the AFM cantilever is ~3 $N \cdot m^{-1}$. The growth was confined at the nucleation stage without sprouting Li whiskers. Note that by increasing the driving potential between the AFM tip and the Li source, the nucleus could resume growth (see Supplementary Fig. 6 and Supplementary Video 3). Scale bar in (**d**) is 200 nm.

Supplementary Discussion: ***Schematic Interpretation of the in situ ETEM observations***

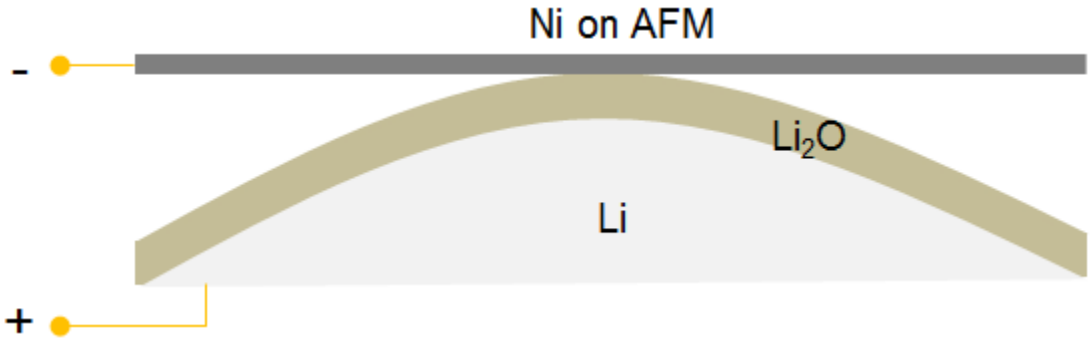

Step 1: Prior to deposition, make contact and apply potential between the "solid electrolyte layer" on the Li metal and Ni current collector on the AFM tip.

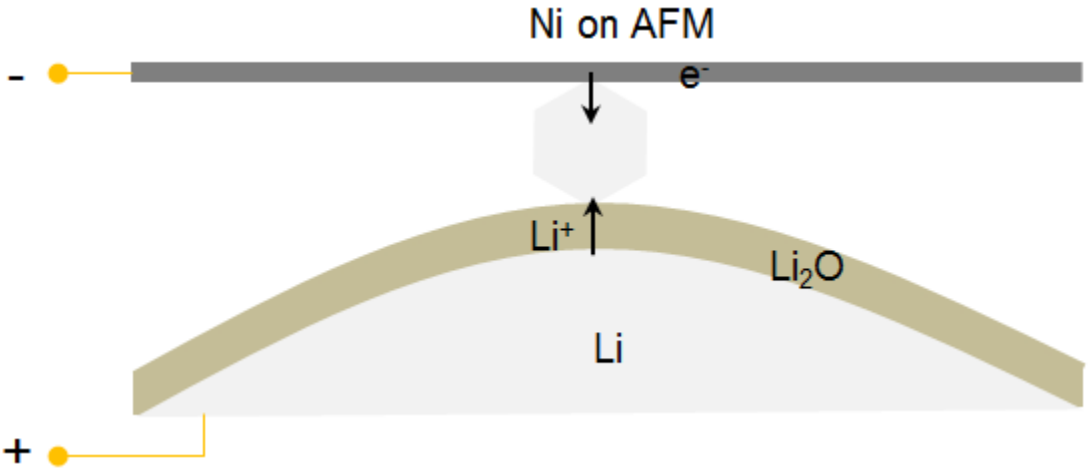

Step 2: Projection view of the Li nanoparticle during the incipient deposition shows a hexagon shape terminated dominantly by {1 1 0} surface facets. Given the fact that the {1 1 0} surface has the minimum surface energy amongst major low-index planes of body-centered cubic Li in CO_2 gas environment, the observed special shape appeared to be dominated by the thermodynamic minimization of surface energies. Therefore, by using Wulff construction, it is expected that 3D geometry of the incipient Li deposition should be a "rhombic decahedron" bounded by {1 1 0} surface facets, the projection of which is consistent with our observation. Since the Li nanoparticle initially grew fast in a relatively low pressure of CO_2, coverage and thickness of the surface reactions products (referred to as "SEI" hereafter, which mainly contains Li_2O, Li_2CO_3, and C) between Li and CO_2 gas molecules are reasonably trivial. Note that scattered events entailing dissociation of CO_2 molecules on Li metal surfaces and injection of O atoms below the Li metal surface are not excluded. As such, the nanoparticle nucleation and incipient growth

can be assisted by Li^0 atoms diffusion on bare Li metal surface and self-diffusion within the nanoparticle, rather than by Li^+ diffusion in "SEI".

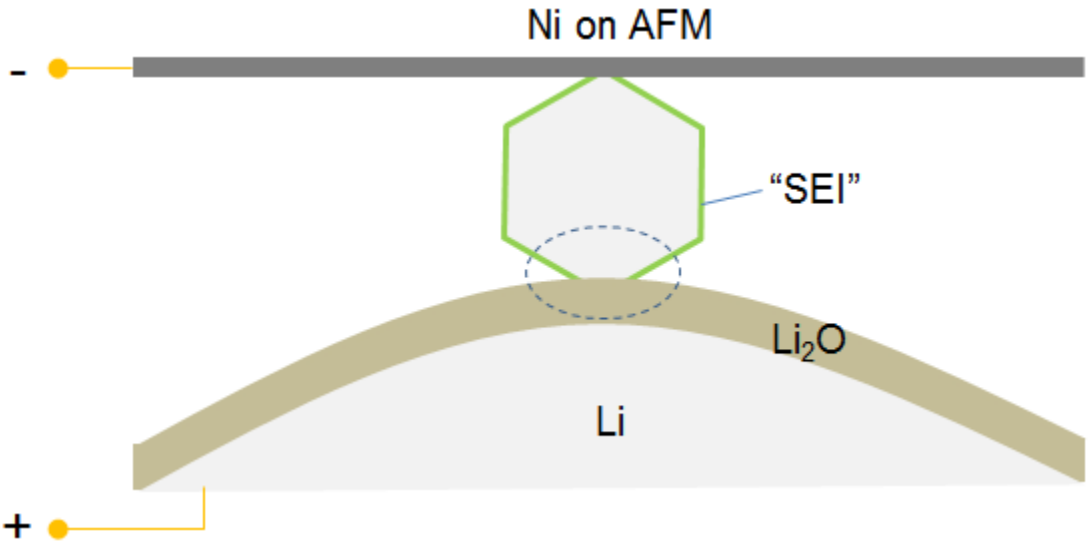

Step 3: Li particle surface areal expansion gradually slows down, since the Li^0 atoms generated at the electrolyte-lithium interface are to be distributed over an expanding surface area of the Li particle. As a result, surface SEI coverage increases and fresh Li surface sites gradually disappear together with the pathway of Li^0 conduction. In the meantime, Li^+ ions conduction pathway was gradually established within the initial "SEI".

The additional particles growth (nearby the contact of the Li particle nucleus and Ni current collector) showing in Supplementary Video 1 (~5s and ~10s) and Fig. 4f can be explained by the conduction of Li^+ ions through and/or on the surface of the "SEI", to the contact of Ni and the Li particle, and subsequent reduction and deposition.

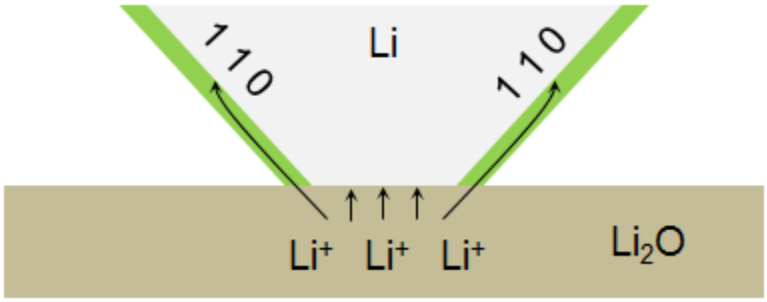

Schematic illustration of the Li^+ ions diffusion pathways at **Step 3**. Li^+ ions preferred to be reduced at the contact, leading to transition from particle growth to whisker growth (see **Step 4**).

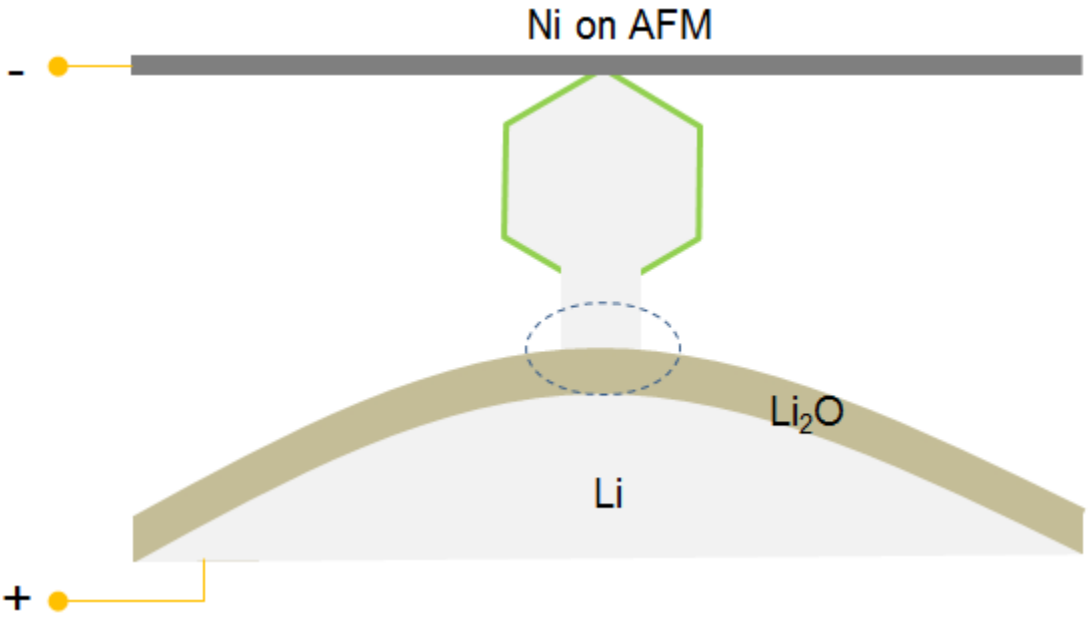

Step 4: The preferential deposition at the contact resulted in a new section of Li (nucleus of Li whisker) which tore open the interface between the "SEI" (green color) and Li_2O solid electrolyte (dark gray) and pushed the Li nanoparticle upward.

Above all, the transition from particle deposition to whisker deposition was initiated by localized deposition of Li. This can be reasonably explained by the fact that, at the instant when bare Li metal surface for Li^0 conduction disappeared, the "SEI" was still too thin and sluggish to carry the Li^+ flux which consequently preferentially deposited at the contact between the Li particle and the Li_2O solid electrolyte. More fundamentally, the transition was due to the lack of Li transport capability on the Li particle surface. Consistent with this fundamental insight, when the surface "SEI" was modified by changing the surrounding gas to N_2 which introduced the highly ionic conductive lithium nitride to the surface, continuous expansion of the Li particle can be achieved in our set-up through continuous deposition on the particle surface.

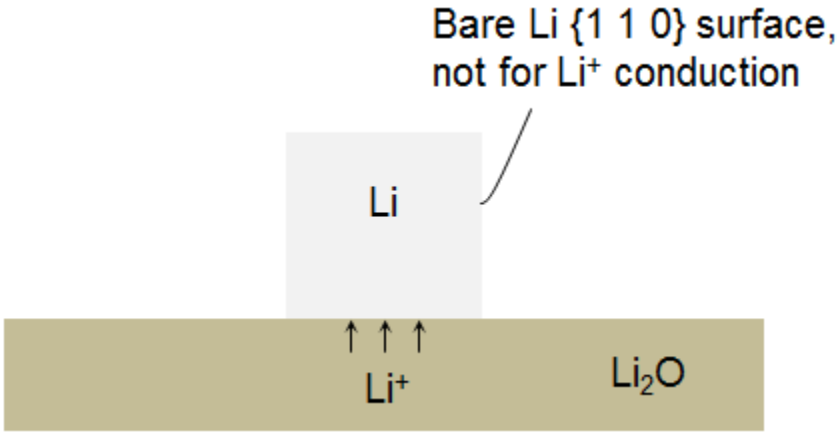

Zoom-in view of the contact in **Step 4** after the nucleation of the whisker section. Due to the short time of exposure to CO_2, there should be trivial "SEI" on the freshly deposited whisker section, and hence conduction of Li^+ ions was trivial on the side surfaces. Therefore, Li^+ ions were collectively reduced to Li^0 atoms at the contact. Given no driving force for the Li^0 atoms diffusion on the side surfaces, the Li^0 atoms largely deposited at the contact, resulting in continuous elongation of the Li whisker.

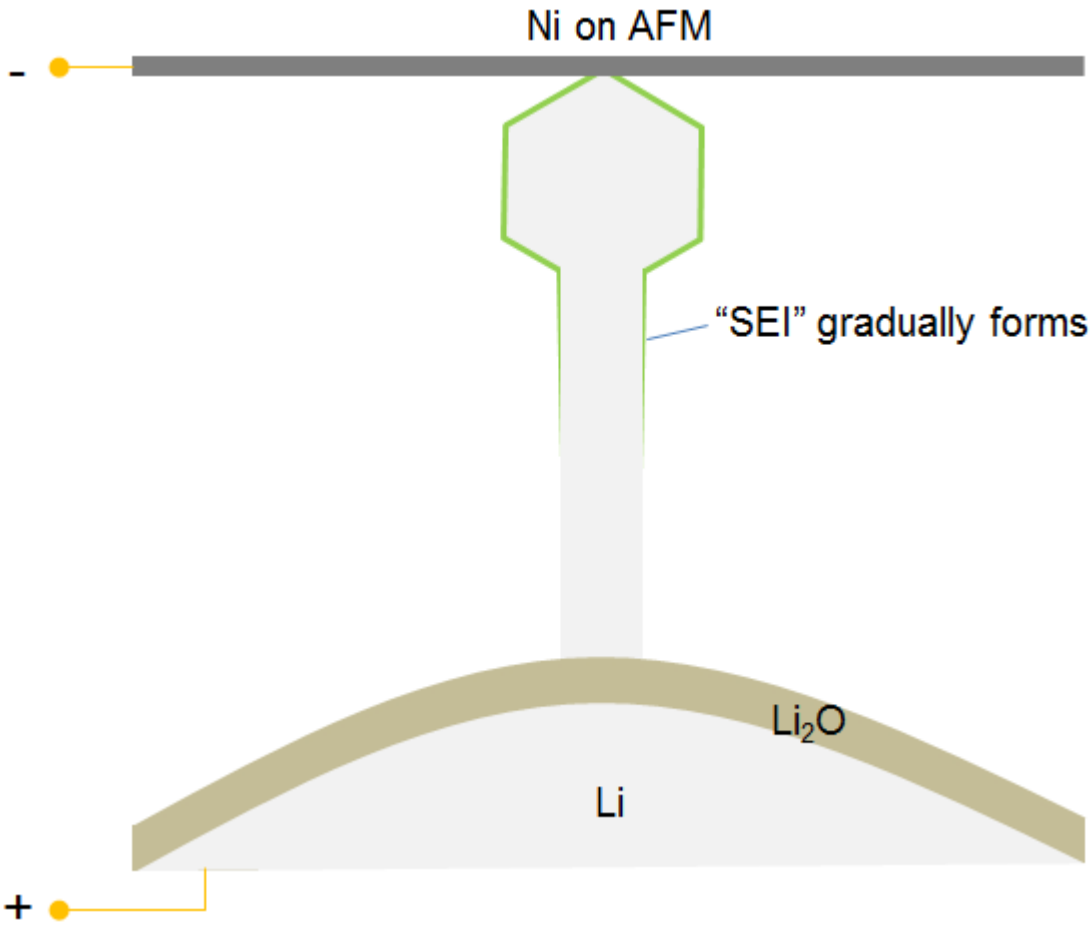

Step 5: The Li whisker kept growing until yielding, buckling, or stop-vertical-elongation. In the meantime, with increasing exposure time to the CO_2 environment in ETEM, the Li whisker was gradually covered by "SEI" (reaction products of CO_2 with the Li metal surface).

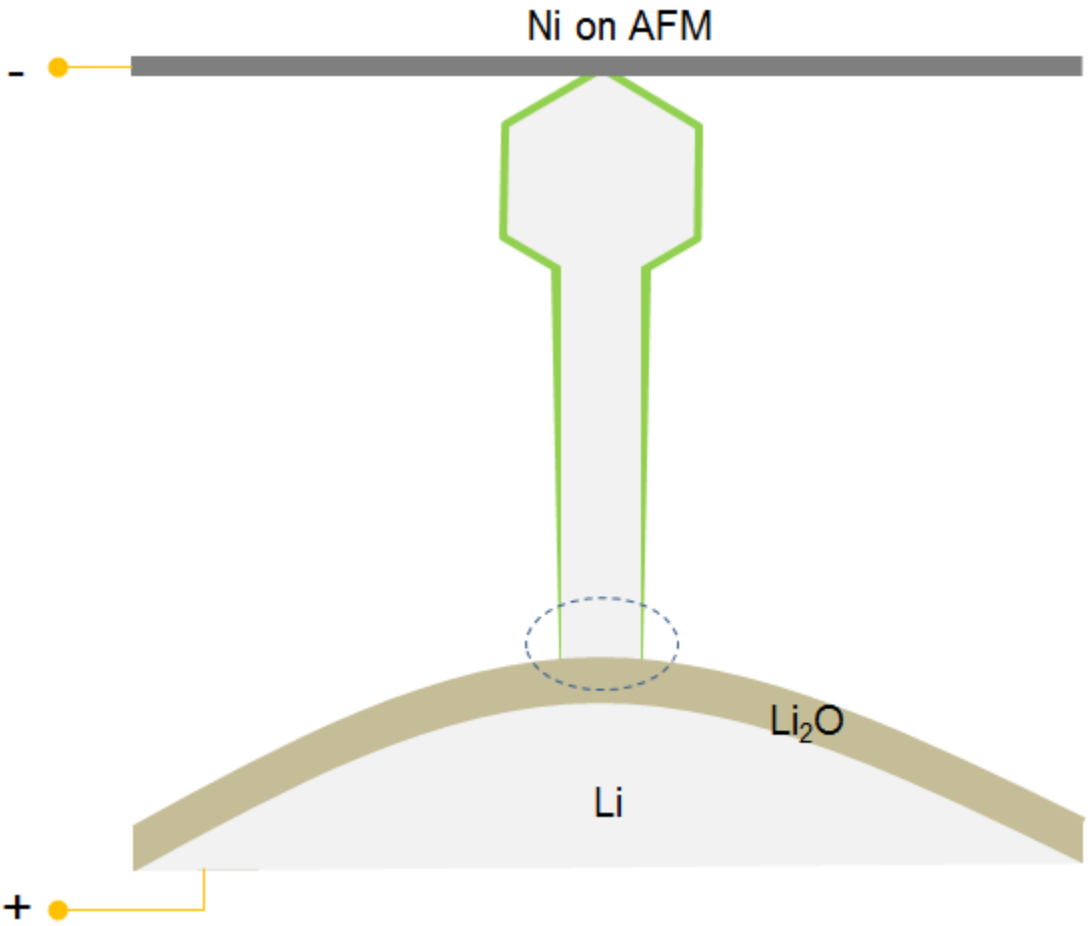

Step 6: Vertical-elongation of the whisker slows down due to high compressive stress at the contact. In the meantime, Li^+ ions conduction through the "SEI" gradually resumes, enabling deposition on the side surfaces and lateral expansion of the Li whisker (see **Step 7**).

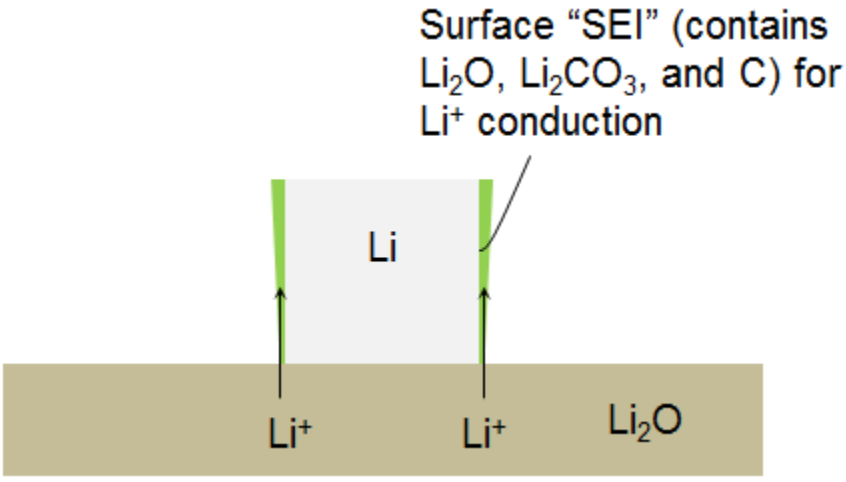

Zoom-in view of the contact at **Step 6** showing increasing Li^+ ion conduction through the "SEI".

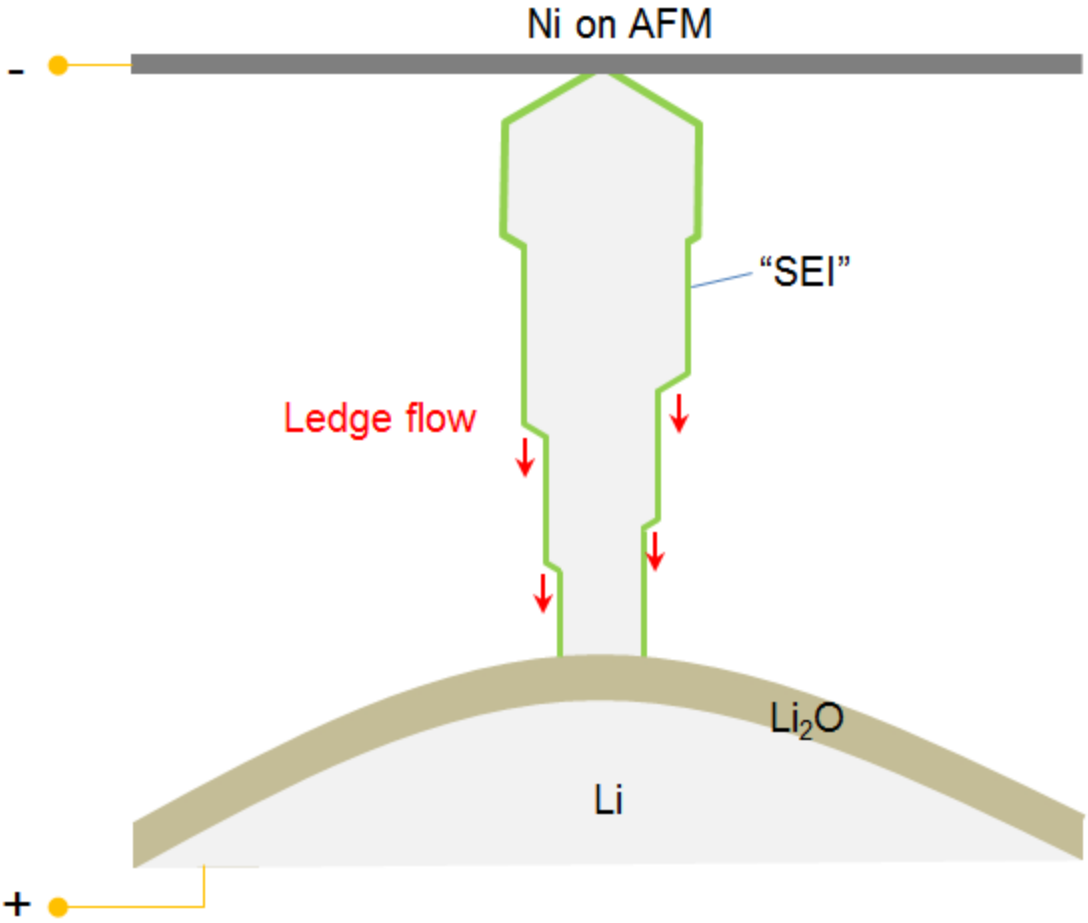

Step 7: Lateral expansion of the whisker mediated by Li^+ ions transport in the "SEI". Surface sites with negative curvature were preferred deposition sites, manifesting a "ledge flow" phenomenon (see Supplementary Video 4_21s and Supplementary Video 5_8s for evidence).

Supplementary Video Captions

Video 1 | *In situ* TEM observation of the Li whisker formation in CO_2 environment.

Video 2 | *In situ* TEM observation of the Li deposition in N_2 environment.

Video 3-4 | *In situ* TEM observation of the Li whisker "failure" by buckling.

Video 5-6 | *In situ* TEM observation of the Li whisker "failure" by cessation of Li deposition on the solid electrolyte-whisker interface.

Video 7 | *In situ* TEM observation of the Li whisker "failure" by kink formation.

Video 8 | *In situ* TEM observation of the Li whisker "failure" by a combined effect of yielding and buckling.